Available online at www.sciencedirect.com
SCIENCE DIRECT®

Computers and Structures 82 (2004) 35–54

Membrane elements insensitive to distortion using the quadrilateral area coordinate method

Xiao-Ming Chen [a], Song Cen [b,*], Yu-Qiu Long [a], Zhen-Han Yao [b]

[a] *Department of Civil Engineering, Tsinghua University, Beijing 100084, China*
[b] *Department of Engineering Mechanics, Tsinghua University, Beijing 100084, China*

Received 24 December 2002; accepted 11 August 2003

Abstract

Two 4-node quadrilateral membrane elements, denoted as AGQ6-I and AGQ6-II, have been developed in this paper. Instead of the traditional isoparametric coordinate, the quadrilateral area coordinates were used to establish the formulations of the new elements. And several generalized conforming conditions were then introduced to determine all unknown parameters. Numerical examples showed that the presented elements exhibit excellent performances in both regular and distorted mesh divisions. They could even yield exact solutions for pure bending problems under distorted meshes and provide lock-free solutions for the MacNeal's test problem of trapezoidal locking. Besides, the weak patch test was conducted to guarantee the convergence of both new elements. It has also been demonstrated that the area coordinate method is an efficient tool for developing simple, effective and reliable serendipity plane membrane elements.

Keywords: Finite element; Quadrilateral area coordinates; Mesh distortion; 4-node quadrilateral element; AGQ6-I; AGQ6-II

1. Introduction

Although the isoparametric coordinates (ξ, η) have been broadly applied in the constructions of quadrilateral membrane elements, such formulation approach still has several disadvantages. For examples, in most of the ordinary cases (i.e., when the shape of the element is not a parallelogram), (1) the isoparametric coordinates (ξ, η) cannot be expressed in terms of the Cartesian coordinates (x, y) in finite terms; (2) The element stiffness matrix contains the determinant of Jacobian inverse, for which the value obtained by numerical integration is usually only an approximation; etc.

Lee and Bathe [1] have studied the influence of mesh distortion on the isoparametric membrane elements and showed that the serendipity family is very sensitive to the mesh distortion. The reasons may be given as follows. The displacement field of a high order serendipity element is expressed with a high order complete polynomial in the isoparametric coordinate system (ξ, η). In the case of a rectangular element, the transformation between (ξ, η) and (x, y) is linear, and the displacement field can also be expressed with a complete polynomial of the same high order in the Cartesian coordinate system (x, y), so the rectangular element usually possesses high precision. In the case of a distorted element, the transformation between (ξ, η) and (x, y) is nonlinear, and the order of the complete polynomial in the Cartesian coordinate system will descend to 1, so the precision of the distorted element is low. That is to say, when the

* Corresponding author. Fax: +86-10-627-81824.
E-mail address: censong@mail.tsinghua.edu.cn (S. Cen).

0045-7949/$ - see front matter
doi:10.1016/j.compstruc.2003.08.004

element is distorted from rectangle to irregular quadrilateral, the transformation between (ξ,η) and (x,y) is changed from linear to nonlinear, then the complete order of (x,y) of displacement field will drop dramatically. This is the explanation why serendipity quadrilateral membrane elements perform badly when they are distorted.

In view of the shortcomings of the isoparametric coordinates mentioned above, a new natural coordinate system, that is, the quadrilateral area coordinate method was proposed in Refs. [2,3]. The quadrilateral area coordinate system possesses an important advantage: the transformation between the area coordinates and the Cartesian coordinates is always linear. Thus, the order of the displacement field expressed by the area coordinates will not vary with the mesh distortion, and as a result, it makes the element insensitive to mesh distortion. Based on the quadrilateral area coordinate method presented in Refs. [2,3], two 8-node membrane elements AQ8-I and AQ8-II, and a 4-node plate-bending element ACGCQ, were successfully developed in Refs. [4,5], respectively. Compared with those traditional models using isoparametric coordinates, these new elements are even less sensitive to mesh distortion.

The sensitive problem for a distorted 4-node quadrilateral membrane element has always attracted many researchers for the past years. MacNeal presented several benchmark problems [6] and the corresponding theorem [7] for checking the trapezoidal locking of the 4-node membrane element. For improving the accuracy and overcoming trapezoidal locking, many approaches have been proposed, such as introducing additional bubble displacement fields and internal degrees of freedom [8,9], the stress hybrid element methods [10–12], the quasi-conforming element method [13], the assumed strain element methods [14,15], and so on. Though all of these skills can enhance the elements' performance more or less, few models can pass the trapezoidal locking test examples proposed in Ref. [6] perfectly.

In order to overcome sensitivity to mesh distortion, the appearance of non-conforming elements seemed to be inevitable. Irons et al. [16,17] proposed a simple approach, namely, patch test, for examining the convergence of the non-conforming elements. This constant strain/stress patch test has been adopted very broadly in finite element analysis, but it also arose many discussions at the same time [18–21]. It usually includes two types: the "strict" form and the "weak" form [22]. The strict patch test is easy to be carried out only using a fixed mesh division, i.e., the number and the sizes of all elements in the mesh will never be changed during the whole procedure. It requests that the element can yield exact solutions under such fixed conditions. Unlike the strict form, the weak patch test does not need exact solutions under a coarse, fixed mesh division. If, as the mesh is repeatedly subdivided, elements come to display the expected state of constant strain/stress, then the element is said to have passed the weak patch test, and convergence to correct results is assured. It is obviously that the thought of the weak patch test is more consistent with the concept of convergence.

The main purpose of this paper is to find an effective way to construct robust elements that are insensitive to the mesh distortion. For this goal, two new 4-node quadrilateral membrane elements, denoted as AGQ6-I and AGQ6-II, are developed. Their displacement fields u and v include four nodal degrees of freedom (DOFs) and two internal DOFs, respectively. And other larruping characters can be listed as follows:

(1) The displacement filed is expressed with the polynomial in area coordinates (instead of the isoparametric coordinates). Thus, whether the element is distorted or not, the order of the complete polynomial in the Cartesian coordinates system (x,y) will not change.
(2) Various generalized conforming conditions [4,5,23–26] are adopted for determining displacement field, including nodal version conforming conditions, and integral form conforming conditions of the displacement along the perimeter of the element.
(3) Only the weak patch test, instead of the strict form, is used to assure the convergence of the elements.
(4) The internal DOFs are condensed during the element analysis level. Therefore, the element stiffness matrix is still an 8×8 matrix after condensation.

2. Area coordinates for quadrilateral elements

As shown in Fig. 1, the position of an arbitrary point P within a quadrilateral element $\overline{1234}$ is specified by the area coordinates L_1, L_2, L_3 and L_4, which are defined as [2,3]:

$$L_i = \frac{A_i}{A} \quad (i = 1,2,3,4) \tag{1}$$

where A is the area of the quadrilateral element; A_i $(i = 1,2,3,4)$ are the areas of the four triangles constructed by point P and four element sides $\overline{23}$, $\overline{34}$, $\overline{41}$ and $\overline{12}$, respectively.

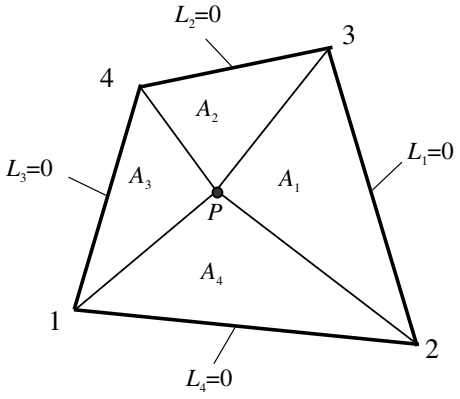

Fig. 1. Definition of the quadrilateral area coordinates L_i.

L_1, L_2, L_3 and L_4 can be expressed in terms of Cartesian coordinates (x, y) as follows:

$$L_i = \frac{1}{2A}(a_i + b_i x + c_i y) \quad (i = 1, 2, 3, 4) \tag{2}$$

where

$$a_i = x_j y_k - x_k y_j, \qquad b_i = y_j - y_k, \qquad c_i = x_k - x_j, \quad \overleftrightarrow{i, j, k} = \overleftrightarrow{1, 2, 3, 4} \tag{3}$$

and (x_i, y_i) $(i = 1, 2, 3, 4)$ are the Cartesian coordinates of the four corner nodes.

The following four dimensionless parameters g_1, g_2, g_3 and g_4 to each of the quadrangles, as shown in Fig. 2. are introduced:

$$g_1 = \frac{A'}{A}, \quad g_2 = \frac{A''}{A}, \quad g_3 = 1 - g_1, \quad g_4 = 1 - g_2 \tag{4}$$

where A' and A'' are the areas of $\Delta 124$ and $\Delta 123$, respectively.

It is obvious that any point in a plane problem has two DOFs. Therefore, only two of the coordinates L_i $(i = 1, 2, 3, 4)$ are independent. It can be shown that L_i $(i = 1, 2, 3, 4)$ must satisfy [2] the following conditions:

$$L_1 + L_2 + L_3 + L_4 = 1 \tag{5}$$

$$g_4 g_1 L_1 - g_1 g_2 L_2 + g_2 g_3 L_3 - g_3 g_4 L_4 = 0 \tag{6}$$

Note that L_i $(i = 1, 2, 3, 4)$ can also be expressed in terms of the quadrilateral isoparametric coordinates (ξ, η) as follows:

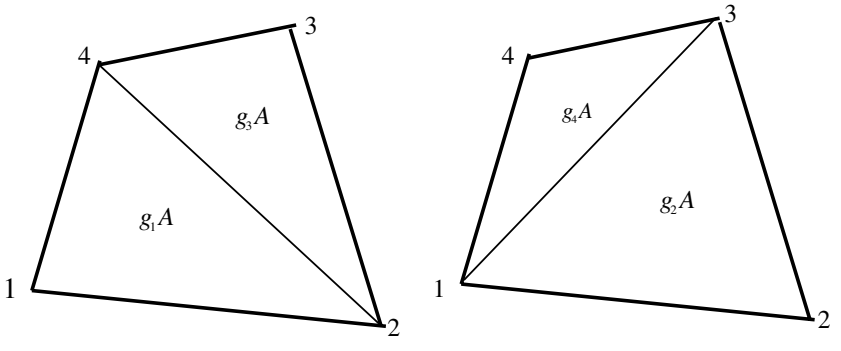

Fig. 2. Definition of the four parameters g_1, g_2, g_3 and g_4.

$$
\begin{aligned}
L_1 &= \frac{1}{4}(1-\xi)[g_2(1-\eta)+g_3(1+\eta)]\\
L_2 &= \frac{1}{4}(1-\eta)[g_4(1-\xi)+g_3(1+\xi)]\\
L_3 &= \frac{1}{4}(1+\xi)[g_1(1-\eta)+g_4(1+\eta)]\\
L_4 &= \frac{1}{4}(1+\eta)[g_1(1-\xi)+g_2(1+\xi)]
\end{aligned}
\tag{7}
$$

The area coordinates of four corner nodes are

1: $(g_2, g_4, 0, 0)$ 2: $(0, g_3, g_1, 0)$ 3: $(0, 0, g_4, g_2)$ 4: $(g_3, 0, 0, g_1)$

In a quadrilateral element, the following basic formulae can be used to evaluate the line integral for arbitrary power functions of area coordinates along each side $L_i = 0$ $(i = 1, 2, 3, 4)$:

(i) Along side $\overline{12}$ $(L_4 = 0)$

$$\int_0^1 L_1^m L_2^n L_3^p \,\mathrm{d}\bar{s} = \frac{m!n!p!}{(m+n+p+1)!} g_2^m g_1^p \sum_{k=0}^{n} g_3^{n-k} g_4^k C_{p+n-k}^p C_{m+k}^m \tag{8a}$$

(ii) Along side $\overline{23}$ $(L_1 = 0)$

$$\int_0^1 L_2^n L_3^p L_4^q \,\mathrm{d}\bar{s} = \frac{n!p!q!}{(n+p+q+1)!} g_3^n g_2^q \sum_{k=0}^{p} g_4^{p-k} g_1^k C_{q+p-k}^q C_{n+k}^n \tag{8b}$$

(iii) Along side $\overline{34}$ $(L_2 = 0)$

$$\int_0^1 L_3^p L_4^q L_1^m \,\mathrm{d}\bar{s} = \frac{p!q!m!}{(p+q+m+1)!} g_4^p g_3^m \sum_{k=0}^{q} g_1^{q-k} g_2^k C_{m+q-k}^m C_{p+k}^p \tag{8c}$$

(iv) Along side $\overline{41}$ $(L_3 = 0)$

$$\int_0^1 L_4^q L_1^m L_2^n \,\mathrm{d}\bar{s} = \frac{q!m!n!}{(q+m+n+1)!} g_1^q g_4^n \sum_{k=0}^{m} g_2^{m-k} g_3^k C_{n+m-k}^n C_{q+k}^q \tag{8d}$$

where $\bar{s}$ is a dimensionless coordinate along each side, and it is 0 at the starting node and 1 at ending node; m, n, p and q are arbitrary positive integers; and C_m^n is defined as

$$C_m^n = \frac{m!}{(m-n)!n!} \tag{9}$$

And two equivalent basic integral formulae, which can be used to evaluate the area integrals for the arbitrary power function of area co-ordinates, are given as follows:

$$
\begin{aligned}
\int\int_A L_1^m L_2^n L_3^p L_4^q \,\mathrm{d}A = \frac{m!n!p!q!}{(m+n+p+q+2)!} \cdot 2A \cdot \Bigg[& g_3^{m+n+1} \sum_{k=0}^{q} \sum_{j=0}^{p} C_{m+q-k}^m C_{n+p-j}^n C_{k+j}^k g_2^k g_4^j g_1^{p+q-k-j} \\
& + g_1^{p+q+1} \sum_{k=0}^{m} \sum_{j=0}^{n} C_{m+q-k}^q C_{n+p-j}^p C_{k+j}^k g_2^k g_4^j g_3^{m+n-k-j} \Bigg]
\end{aligned}
\tag{10a}
$$

$$
\begin{aligned}
\int\int_A L_1^m L_2^n L_3^p L_4^q \,\mathrm{d}A = \frac{m!n!p!q!}{(m+n+p+q+2)!} \cdot 2A \cdot \Bigg[& g_4^{n+p+1} \sum_{k=0}^{m} \sum_{j=0}^{q} C_{n+m-k}^n C_{p+q-j}^p C_{k+j}^k g_3^k g_1^j g_2^{m+q-k-j} \\
& + g_2^{m+q+1} \sum_{k=0}^{n} \sum_{j=0}^{p} C_{m+n-k}^m C_{q+p-j}^q C_{k+j}^k g_3^k g_1^j g_4^{n+p-k-j} \Bigg]
\end{aligned}
\tag{10b}
$$

3. Formulations of the element AGQ6-I

3.1. Element nodal displacement vector $\{\mathbf{q}\}^e$ and internal parameter vector $\{\boldsymbol{\lambda}\}^e$

Consider the quadrilateral element shown in Fig. 3, the element nodal displacement vector $\{\mathbf{q}\}^e$ is given by

$$\{\mathbf{q}\}^e = [\,u_1 \quad v_1 \quad u_2 \quad v_2 \quad u_3 \quad v_3 \quad u_4 \quad v_4\,]^T \tag{11}$$

In addition, the displacement field u is assumed to include two internal parameters λ_1 and λ_2, and v is also assumed to include two internal parameters λ_1' and λ_2'. These four parameters form the internal parameter vector $\{\boldsymbol{\lambda}\}^e$

$$\{\boldsymbol{\lambda}\}^e = [\,\lambda_1 \quad \lambda_1' \quad \lambda_2 \quad \lambda_2'\,]^T \tag{12}$$

Thus, the displacement fields of the element can be expressed by the sum of $\{\mathbf{q}\}^e$ and $\{\boldsymbol{\lambda}\}^e$.

$$\begin{Bmatrix} u \\ v \end{Bmatrix} = \begin{Bmatrix} u^0 \\ v^0 \end{Bmatrix} + \begin{Bmatrix} u_\lambda \\ v_\lambda \end{Bmatrix} = [\mathbf{N}_q]\{\mathbf{q}\}^e + [\mathbf{N}_\lambda]\{\boldsymbol{\lambda}\}^e \tag{13}$$

where u^0 and v^0 are the essential displacement fields related to $\{\mathbf{q}\}^e$; u_λ and v_λ are the additional internal displacement fields related to $\{\boldsymbol{\lambda}\}^e$;

$$[\mathbf{N}_q] = \begin{bmatrix} N_1^0 & 0 & N_2^0 & 0 & N_3^0 & 0 & N_4^0 & 0 \\ 0 & N_1^0 & 0 & N_2^0 & 0 & N_3^0 & 0 & N_4^0 \end{bmatrix} \tag{14}$$

$$[\mathbf{N}_\lambda] = \begin{bmatrix} N_{\lambda 1} & 0 & N_{\lambda 2} & 0 \\ 0 & N_{\lambda 1} & 0 & N_{\lambda 2} \end{bmatrix} \tag{15}$$

which are the shape function matrix and the internal parameter shape function matrix, respectively.

3.2. Shape functions N_i^0

The shape functions for u^0 and v^0 have the same forms. So only the derivation of u^0 is given as follows.
Let u^0 be the second-order polynomial in terms of the area coordinates L_i $(i = 1, 2, 3, 4)$

$$u^0 = \alpha_1 + \alpha_2(L_3 - L_1) + \alpha_3(L_4 - L_2) + \alpha_4(L_3 - L_1)(L_4 - L_2) \tag{16}$$

where α_1, α_2, α_3 and α_4 are four unknown constants. In order to determine these four constants, four generalized conforming conditions are introduced, i.e.

$$\sum_{i=1}^{4}(u^0 - \tilde{\boldsymbol{u}})_i = 0, \quad \sum_{i=1}^{4}(u^0 - \tilde{\boldsymbol{u}})_i\xi_i\eta_i = 0, \quad \oint_{\partial A} \bar{l}(u^0 - \tilde{\boldsymbol{u}})\,\mathrm{d}s = 0, \quad \oint_{\partial A} \bar{m}(u^0 - \tilde{\boldsymbol{u}})\,\mathrm{d}s = 0 \tag{17}$$

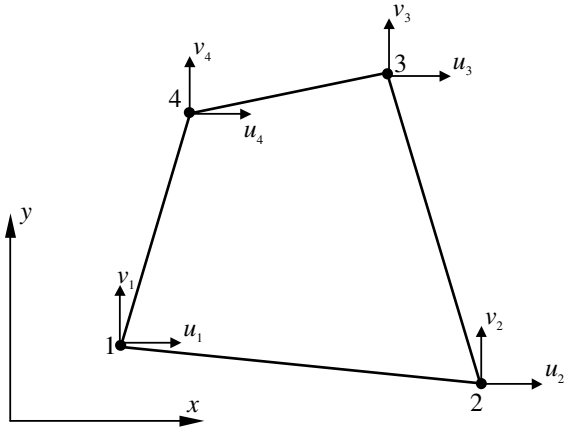

Fig. 3. A 4-node quadrilateral membrane element.

where the first two are the combination forms of the nodal conforming conditions, and the other two are the integral form conforming conditions along the perimeter ∂A of the element; $\tilde{\boldsymbol{u}}$ is the displacement at the element boundary; $\overline{l}$ and $\overline{m}$ are the direction cosines of the outer normal along the element boundary.

Then, the shape functions N_i^0 $(i = 1, 2, 3, 4)$ can be obtained from equation (17):

$$N_i^0 = -\frac{g_k}{2} + L_i + L_j + \xi_i \eta_i g_k P \quad (i = 1, 2, 3, 4;\ j = 2, 3, 4, 1;\ k = 3, 4, 1, 2) \tag{18}$$

with

$$P = \frac{3(L_3 - L_1)(L_4 - L_2) - (g_2 - g_3)(L_3 - L_1) - (g_1 - g_2)(L_4 - L_2) - \frac{1}{2}(g_2 g_4 - g_1 g_3)}{1 + g_1 g_3 + g_2 g_4} \tag{19}$$

3.3. Internal parameter shape functions $N_{\lambda i}$

The shape functions of the internal displacement fields are given by

$$\begin{aligned} N_{\lambda 1} &= L_1 L_3 \\ N_{\lambda 2} &= L_2 L_4 \end{aligned} \tag{20}$$

It can be seen that the nodal values of these two shape functions are both zero. When the element shape degenerates to rectangle, $N_{\lambda i}$ $(i = 1, 2)$ will be the same as the internal parameter shape functions of the element Q6 proposed by Wilson et al. [8].

3.4. Element stiffness matrix

Substitution of Eqs. (18) and (20) into (13) yields the displacement fields. It can be shown that such displacement fields are the complete second-order polynomial in terms of the Cartesian coordinates (x, y).

Then, by utilizing the transformation of derivatives of first order [3]:

$$\begin{Bmatrix} \dfrac{\partial}{\partial x} \\ \dfrac{\partial}{\partial y} \end{Bmatrix} = \frac{1}{2A} \begin{bmatrix} b_1 & b_2 & b_3 & b_4 \\ c_1 & c_2 & c_3 & c_4 \end{bmatrix} \begin{Bmatrix} \dfrac{\partial}{\partial L_1} \\ \dfrac{\partial}{\partial L_2} \\ \dfrac{\partial}{\partial L_3} \\ \dfrac{\partial}{\partial L_4} \end{Bmatrix} \tag{21}$$

the element strain vector $\{\boldsymbol{\varepsilon}\}^{\mathrm{e}}$ can be obtained:

$$\{\boldsymbol{\varepsilon}\}^{\mathrm{e}} = [\mathbf{B}_q]\{\mathbf{q}\}^{\mathrm{e}} + [\mathbf{B}_\lambda]\{\boldsymbol{\lambda}\}^{\mathrm{e}} \tag{22}$$

where

$$\{\boldsymbol{\varepsilon}\}^{\mathrm{e}} = [\,\varepsilon_x \quad \varepsilon_y \quad \gamma_{xy}\,]^T \tag{23}$$

$$[\mathbf{B}_q] = [\,[\mathbf{B}_{q1}] \quad [\mathbf{B}_{q2}] \quad [\mathbf{B}_{q3}] \quad [\mathbf{B}_{q4}]\,] \tag{24}$$

with

$$[\mathbf{B}_{qi}] = \begin{bmatrix} \dfrac{\partial N_i^0}{\partial x} & 0 \\ 0 & \dfrac{\partial N_i^0}{\partial y} \\ \dfrac{\partial N_i^0}{\partial y} & \dfrac{\partial N_i^0}{\partial x} \end{bmatrix} \quad (i = 1, 2, 3, 4) \tag{25}$$

and

$$\begin{aligned}\frac{\partial N_i^0}{\partial x} &= \frac{b_i}{2A}+\frac{b_j}{2A}+\frac{\xi_i\eta_i g_k}{2A(1+g_1g_3+g_2g_4)}S_x\\ \frac{\partial N_i^0}{\partial y} &= \frac{c_i}{2A}+\frac{c_j}{2A}+\frac{\xi_i\eta_i g_k}{2A(1+g_1g_3+g_2g_4)}S_y\end{aligned}\quad (i=1,2,3,4;\ j=2,3,4,1;\ k=3,4,1,2) \tag{26a}$$

$$\begin{aligned}S_x &= \textstyle\sum_{i'=1}^4 b_{i'}\xi_{i'}\eta_{i'}[3(L_{j'}-L_{m'})+(g_{j'}-g_{k'})]\\ S_y &= \textstyle\sum_{i'=1}^4 c_{i'}\xi_{i'}\eta_{i'}[3(L_{j'}-L_{m'})+(g_{j'}-g_{k'})]\end{aligned}\quad \begin{pmatrix} i'=\overleftrightarrow{1,2,3,4} & j'=\overleftrightarrow{2,3,4,1}\\ k'=\overleftrightarrow{3,4,1,2} & m'=\overleftrightarrow{4,1,2,3}\end{pmatrix} \tag{26b}$$

$$[\mathbf{B}_\lambda]=[\,[\mathbf{B}_{\lambda 1}]\quad [\mathbf{B}_{\lambda 2}]\,] \tag{27}$$

with

$$[\mathbf{B}_{\lambda i}]=\begin{bmatrix}\dfrac{\partial N_{\lambda i}}{\partial x} & 0\\ 0 & \dfrac{\partial N_{\lambda i}}{\partial y}\\ \dfrac{\partial N_{\lambda i}}{\partial y} & \dfrac{\partial N_{\lambda i}}{\partial x}\end{bmatrix}\quad (i=1,2) \tag{28}$$

and

$$\begin{aligned}\frac{\partial N_{\lambda i}}{\partial x} &= \frac{b_i}{2A}L_{i+2}+\frac{b_{i+2}}{2A}L_i\\ \frac{\partial N_{\lambda i}}{\partial y} &= \frac{c_i}{2A}L_{i+2}+\frac{c_{i+2}}{2A}L_i\end{aligned}\quad (i=1,2) \tag{29}$$

After condensation [8], the element stiffness matrix of the element can be expressed by

$$[\mathbf{K}]^{\mathrm{e}}=[\mathbf{K}_{qq}]-[\mathbf{K}_{\lambda q}]^T[\mathbf{K}_{\lambda\lambda}]^{-1}[\mathbf{K}_{\lambda q}] \tag{30}$$

with

$$\begin{aligned}[\mathbf{K}_{qq}] &= \int\int_A [\mathbf{B}_q]^T[\mathbf{D}][\mathbf{B}_q]t\,\mathrm{d}A\\ [\mathbf{K}_{\lambda\lambda}] &= \int\int_A [\mathbf{B}_\lambda]^T[\mathbf{D}][\mathbf{B}_\lambda]t\,\mathrm{d}A\\ [\mathbf{K}_{\lambda q}] &= \int\int_A [\mathbf{B}_\lambda]^T[\mathbf{D}][\mathbf{B}_q]t\,\mathrm{d}A\end{aligned} \tag{31}$$

where t is the thickness of element; $[\mathbf{D}]$ is the elasticity matrix

$$[\mathbf{D}]=\frac{E}{1-\mu^2}\begin{bmatrix}1 & \mu & 0\\ \mu & 1 & 0\\ 0 & 0 & \dfrac{1-\mu}{2}\end{bmatrix} \tag{32}$$

where E and μ are Young's modulus and Poisson's ratio, respectively. For plane strain problems, the E and μ in Eq. (32) should be replaced by $E/(1-\mu^2)$ and $\mu/(1-\mu)$, respectively.

By using the integration formulae equation (10), the explicit expression of $[\mathbf{K}]^{\mathrm{e}}$ can be obtained. However, the numerical integration method would be more convenient for computer coding. Thus, by using Eq. (7), Eq. (31) can be expressed in terms of isoparametric coordinates as follows:

$$\begin{aligned}[\mathbf{K}_{qq}] &= \int_{-1}^1\int_{-1}^1 [\mathbf{B}_q]^T[\mathbf{D}][\mathbf{B}_q]t|\mathbf{J}|\,\mathrm{d}\xi\,\mathrm{d}\eta\\ [\mathbf{K}_{\lambda\lambda}] &= \int_{-1}^1\int_{-1}^1 [\mathbf{B}_\lambda]^T[\mathbf{D}][\mathbf{B}_\lambda]t|\mathbf{J}|\,\mathrm{d}\xi\,\mathrm{d}\eta\\ [\mathbf{K}_{\lambda q}] &= \int_{-1}^1\int_{-1}^1 [\mathbf{B}_\lambda]^T[\mathbf{D}][\mathbf{B}_q]t|\mathbf{J}|\,\mathrm{d}\xi\,\mathrm{d}\eta\end{aligned} \tag{33}$$

where $|\mathbf{J}|$ is the Jacobian determinant, which is the same as that of the 4-node isoparametric element Q4. Since there are no $|\mathbf{J}|^{-1}$ (the Jacobian inverse) in $[\mathbf{B}_q]$ and $[\mathbf{B}_\lambda]$, exact value of $[\mathbf{K}]^e$ can be determined by numerical integration when the 3×3 Gauss integration points are employed.

The new element obtained is named AGQ6-I.

4. Formulations of the element AGQ6-II

The construction procedure of the element AGQ6-II is similar to that of AGQ6-I. The only difference is the expression of their shape functions.

The displacement u^0 of the element AGQ6-II is still given by Eq. (16). But the conforming conditions are changed to the following combination conditions at the element nodes:

$$\sum_{i=1}^{4}(u^0-\tilde{u})_i=0,\quad \sum_{i=1}^{4}(u^0-\tilde{u})_i\xi_i=0,\quad \sum_{i=1}^{4}(u^0-\tilde{u})_i\eta_i=0,\quad \sum_{i=1}^{4}(u^0-\tilde{u})_i\xi_i\eta_i=0 \tag{34}$$

Substitution of Eq. (16) into Eq. (34) yields

$$\begin{aligned}
&\sum_{i=1}^{4}u_i=4\alpha_1+2(g_1-g_2)\alpha_2+2(g_2-g_3)\alpha_3+2(g_2g_4-g_1g_3)\alpha_4\\
&\sum_{i=1}^{4}u_i\xi_i=2\alpha_2\\
&\sum_{i=1}^{4}u_i\eta_i=2\alpha_3\\
&\sum_{i=1}^{4}u_i\xi_i\eta_i=2(g_3-g_2)\alpha_2+2(g_2-g_1)\alpha_3+2(g_2g_4+g_1g_3)\alpha_4
\end{aligned} \tag{35}$$

Then, the shape functions of the element AGQ6-II can be obtained:

$$N_i^0=-\frac{g_k}{2}+L_i+L_j+\xi_i\eta_ig_k\overline{P}\quad(i=1,2,3,4;\ j=2,3,4,1;\ k=3,4,1,2) \tag{36}$$

with

$$\overline{P}=\frac{1}{g_2g_4+g_1g_3}[(L_3-L_1)(L_4-L_2)-\frac{1}{2}(g_2g_4-g_1g_3)] \tag{37}$$

The derivatives of N_i^0 respect to x and y are given by

$$\begin{aligned}
\frac{\partial N_i^0}{\partial x}&=\frac{b_i}{2A}+\frac{b_j}{2A}+\frac{\xi_i\eta_ig_k}{2A(g_1g_3+g_2g_4)}\bar{S}_x\\
\frac{\partial N_i^0}{\partial y}&=\frac{c_i}{2A}+\frac{c_j}{2A}+\frac{\xi_i\eta_ig_k}{2A(g_1g_3+g_2g_4)}\bar{S}_y
\end{aligned}\quad(i=1,2,3,4;\ j=2,3,4,1;\ k=3,4,1,2) \tag{38a}$$

$$\begin{aligned}
\bar{S}_x&=\textstyle\sum_{i'=1}^{4}b_{i'}\xi_{i'}\eta_{i'}(L_{j'}-L_{m'})\\
\bar{S}_y&=\textstyle\sum_{i'=1}^{4}c_{i'}\xi_{i'}\eta_{i'}(L_{j'}-L_{m'})
\end{aligned}\quad\left(i'=\overleftrightarrow{1,2,3,4};\ j'=\overleftrightarrow{2,3,4,1};\ m'=\overleftrightarrow{4,1,2,3}\right) \tag{38b}$$

Substitution of Eq. (38) into (24) yields the matrix $[\mathbf{B}_q]$ of the element AGQ6-II. And other formulations of the element AGQ6-II are the same as those of the element AGQ6-I.

5. Numerical examples

Eight benchmark problems, which are listed in Table 1, have been used to evaluate the performance of the elements AGQ6-I and AGQ6-II. Among these examples, the sixth and seventh ones are two well-known severe examinations for testing the sensitivity to mesh distortion of the quadrilateral elements. The results solved by other 16 element models listed in Table 2 are also given for comparison.

Table 1
List of eight benchmark problems

	Benchmark problems, figure number	Results
1	Beam divided by five quadrilateral elements, Fig. 4	Table 3
2	Beam divided by four quadrilateral elements, Fig. 5	Table 4
3	Cook's skew beam problem, Fig. 6	Table 5
4	Thick curving beam, Fig. 7	Table 6
5	Thin curving beam, Fig. 8	Table 7
6	MacNeal's thin beam with distorted mesh, Fig. 9	Table 8
7	Beam divided by two elements with distortion parameter, Fig. 10	Table 9
8	Weak patch test of constant strain problem, Fig. 11	Table 10

Table 2
List of element models for comparison

No.	Symbols	Elements for comparison	References
1	Q4	4-node isoparametric element	
2	QUAD4	4-node element in MSC/NASTRAN	[6]
3	Q6	4-node isoparametric element with internal parameters	[8]
4	QM6	4-node isoparametric element with internal parameters	[9]
5	P-S	Stress hybrid element	[10]
6	NQ6	Hybrid element	[11]
7	RGD20	Refined hybrid element	[12]
8	QC6	Quasi-conforming element	[13]
9	PEAS7	Assumed strain element	[14]
10	QE2	Assumed strain element	[15]
11	$\bar{B}$-Q4E	Assumed strain element	[15]
12	HL	4-node isoparametric element with internal parameters	[27]
13	PN340	PN element	[28]
14	ANSYS		Commercial program
15	D-type	Membrane element with drilling DOFs	[29]
16	Q4S	Membrane element with drilling DOFs	[30]

Example 1. Cantilever beam divided by five quadrilateral elements (Fig. 4)

The cantilever beam, as shown in Fig. 4, is divided by five irregular quadrilateral elements. And two loading cases are considered: (a) pure bending under moment M; (b) linear bending under transverse force P. The Young's modulus $E = 1500$, Poisson's ratio $\mu = 0.25$. The results of the vertical deflection v_A at point A and the stress σ_{xB} at point B are given in Table 3.

Compared with the results solved by other element models, it can be seen from Table 3 that the new elements AGQ6-I and AGQ6-II give the best answers. Furthermore, exact solutions can even be obtained by the presented elements for the pure bending case.

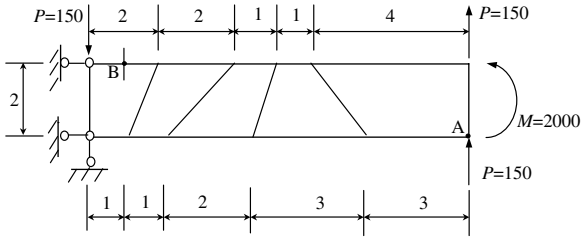

Fig. 4. Cantilever beam with five irregular elements.

Table 3
The deflections and stresses at selected locations for bending problems of a cantilever beam (Fig. 4)

Elements	Load M		Load P	
	v_A	σ_{xB}	v_A	σ_{xB}
Q4	45.7	−1761	50.7	−2448
Q6	98.4	−2428	100.4	−3354
QC6	96.1	−2439	98.1	−3339
NQ6	96.1	−2439	98.0	−3294
QM6	96.07	−2497	97.98	−3235
P-S	96.18	−3001	98.05	−3899
QE-2	96.5	−3004	98.26	−3906
$\overline{B}$-Q4E	96.5	−3004	98.26	−3906
AGQ6-I	100.0	−3000	102.0	−4151
AGQ6-II	100.0	−3000	102.7	−4180
Exact	100.0	−3000	102.6	−4050

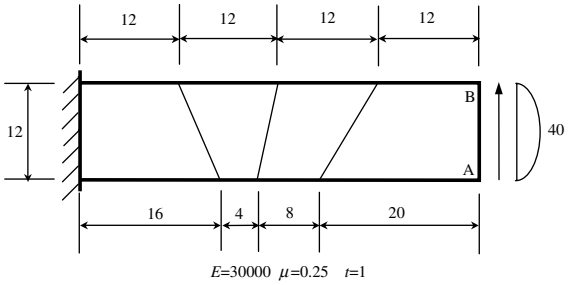

Fig. 5. Cantilever beam with four irregular elements.

Example 2. Cantilever beam divided by four quadrilateral elements (Fig. 5)

As shown in Fig. 5, the cantilever beam is divided by four irregular quadrilateral elements. The results of the deflections at the tip points A and B are shown in Table 4.

From the Table 4, it can be seen again that the two present elements possess the best precisions, and even better than the elements D-type and Q4S with vertex drilling DOFs (the total DOF number of the elements D-type or Q4S is 12 because of the additional vertex drilling DOFs).

Example 3. Cook's skew beam problem (Fig. 6)

This example, in which a skew cantilever with shear distributed load at the free edge, as shown in Fig. 6, was proposed by Cook et al. [22]. The results of vertical deflection at point C, the maximum principal stress at point A and the minimum principal stress at point B are listed in Table 5. Compared with the other elements, the present elements exhibit the best convergence.

Table 4
The deflections at selected locations for bending problem of a cantilever beam (Fig. 5)

Element	Tip deflections			Normalized values		
	Point A	Point B	Average	Point A	Point B	Average
Q4	0.2126	0.2131	0.2129	0.598	0.599	0.598
D-type	–	–	0.3065	–	–	0.861
Q4S	–	–	0.2978	–	–	0.837
AQ6-I	0.3510	0.3509	0.3510	0.987	0.986	0.987
AQ6-II	0.3535	0.3530	0.3533	0.994	0.992	0.993
Reference value		0.3558			1.000	

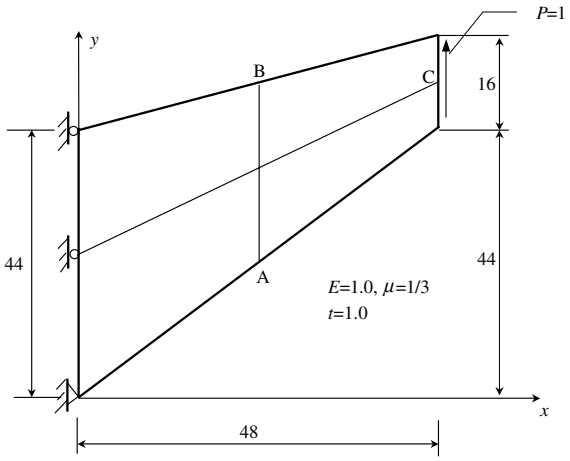

Fig. 6. Cook's skew beam problem.

Table 5
Results of Cook's skew beam (Fig. 6)

Element	v_C				$\sigma_{A\max}$				$\sigma_{B\min}$			
	2×2	4×4	8×8	16×16	2×2	4×4	8×8	16×16	2×2	4×4	8×8	16×16
Q4	11.80	18.29	22.08	23.43	0.1217	0.1873	0.2242	0.2311	−0.0960	−0.1524	−0.1869	−0.1966
Q6	22.94	23.48	23.80	23.91	0.2029	0.2258	0.2334	0.2361	−0.1734	−0.1915	−0.1997	−0.2028
QM6	21.05	23.02	–	–	0.1928	0.2243	–	–	−0.1580	−0.1856	–	–
HL	18.17	22.03	23.39	–	0.1582	0.1980	–	–	−0.1335	−0.1770	–	–
P-S	21.13	23.02	–	23.88	0.1854	0.2241	–	0.2364	–	–	–	–
QE-2	21.35	23.04	–	23.88	0.1956	0.2261	–	0.2364	–	–	–	–
$\overline{B}$-4E	21.35	23.04	–	23.88	0.1956	0.2261	–	0.2364	–	–	–	–
AGQ6-I	23.07	23.68	23.87	23.93	0.2023	0.2275	0.2351	0.2365	−0.1758	−0.1972	−0.2016	−0.2033
AGQ6-II	25.92	24.37	24.04	23.97	0.2169	0.2286	0.2352	0.2365	−0.1999	−0.2014	−0.2027	−0.2035
Reference solution[a]	23.96				0.2362				−0.2023			

[a] Results of the element GT9M8 [26] using 64×64 mesh.

Example 4. Thick curving beam (Fig. 7)

A cantilever thick curving beam, which is divided by five elements, is subjected to a transverse force at its tip (Fig. 7). The results of the tip vertical deflection are shown in Table 6. Better solutions can be obtained by AGQ6-I and AGQ6-II than by other elements QM6, P-S and PEAS7.

Example 5. Thin curving beam (Fig. 8)

As shown in Fig. 8, a cantilever thin curving beam is subjected to a transverse force at the tip. And it is also divided by five elements. Two thickness–radius ratios, (i) $h/R = 0.03$ and (ii) $h/R = 0.006$, are considered. The results of the tip displacement, obtained by the elements Q4, Q6, QM6, QUAD4 and the present elements, are listed in Table 7.

Compared with the mesh used in the previous example, the shape of the elements in this example becomes much narrower. The length–width ratio of the elements reaches 10 when $h/R = 0.03$, and will be larger if $h/R = 0.006$. That is to say, the distortion will become more and more serious if the length–width ratio increases. From the Table 7, it can be seen that elements Q4, Q6, QM6 and QUAD4 are very sensitive to the mesh distortion caused by the increase of the length–width ratio. They all suffer from the locking problem. But at the same time, the presented elements, AGQ6-I and AGQ6-II, are insensitive to this kind of distortion.

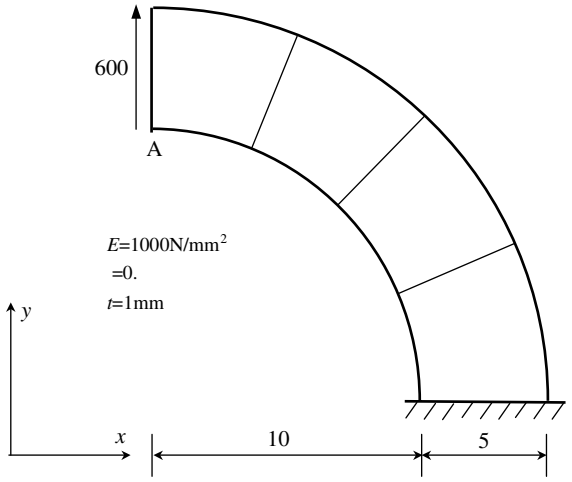

Fig. 7. Bending of thick curving beam.

Table 6
The tip deflection of a thick curving beam (Fig. 7)

Elements	QM6	P-S	PEAS7	AQ6-I	AQ6-II	Exact solution
v_A	83.61	84.58	84.58	91.88	86.93	90.1

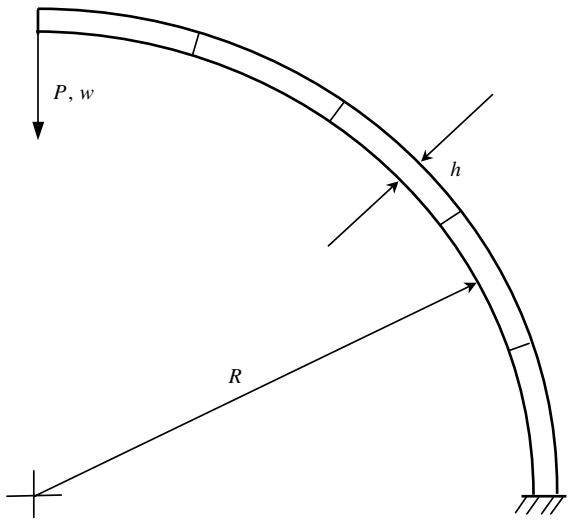

Fig. 8. Bending of thin curving beam.

Table 7
The tip deflection of a thin curving beam (Fig. 8)

h/R	Q4	Q6	QM6	QUAD4	AQ6-I	AQ6-II	Exact solution
0.03	0.024	0.770	0.339	0.615	1.008	1.008	1.000
0.006	0.001	0.285	0.022	0.163	1.008	1.008	1.000

Example 6. MacNeal's thin cantilever beam with distorted meshes (Fig. 9)

Consider the thin beams presented in Fig. 9. Three different mesh shapes, rectangular, parallelogram and trapezoidal, are adopted. This example, proposed by MacNeal and Harder [6], is a famous benchmark for testing the sensitivity to mesh distortion of the 4-node quadrilateral membrane elements. Besides the distortion caused only by the length–width ratio, the composite distortions of parallelogram and trapezoidal shapes together with length–width ratio are also taken into account.

There are two loading cases under consideration: pure bending and transverse linear bending. The Young's modulus of the beam $E = 10^7$; the Poisson's ratio $\mu = 0.3$; and the thickness of the beam $t = 0.1$.

The results of the tip deflection are shown in Table 8. Besides the presented elements, the results obtained by other nine element models are also given for comparison.

From Table 8, one can conclude that

(1) It is obvious that element Q4 suffers from locking problems for all three types of distortion ((a) length–width ratio distortion, (b) parallelogram distortion, (c) trapezoidal distortion) of three different meshes.
(2) Other eight elements can all improve the accuracy more or less.

Firstly, they all exhibit high precision using mesh (a), no locking problem happens for the distortion caused by the length–width ratio.

Secondly, although their precisions are also improved using mesh (b) and mesh (c), the locking problems are still not avoided completely, especially for the trapezoidal locking.

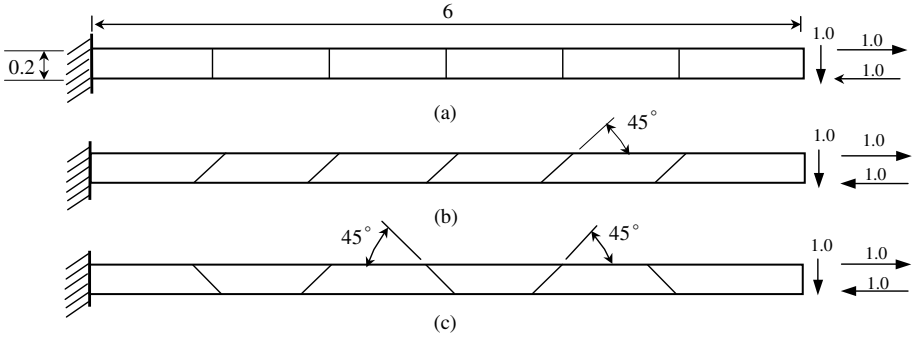

Fig. 9. MacNeal's beam.

Table 8
The normalized results of the tip deflection for the MacNeal's thin beam using different meshes (Fig. 9)

Element	Load P			Load M		
	Mesh (a)	Mesh (b)	Mesh (c)	Mesh (a)	Mesh (b)	Mesh (c)
Q4	0.093	0.035	0.003	0.093	0.031	0.022
Q6	0.993	0.677	0.106	1.000	0.759	0.093
QM6	0.993	0.623	0.044	1.000	0.722	0.037
QUAD4	0.904	0.080	0.071	–	–	–
P-S	0.993	0.798	0.221	1.000	0.852	0.167
PEAS7	0.982	0.795	0.217	–	–	–
PN340	0.982	0.620	0.065	–	–	–
ANSYS	0.979	0.624	0.047	–	–	–
RGD20	0.981	0.625	0.047	–	–	–
AQ6-I	0.993	0.994	0.994	1.000	1.000	1.000
AQ6-II	0.993	0.994	0.994	1.000	1.000	1.000
Exact		1.000[a]			1.000[b]	

[a] The standard value is −0.1081.
[b] The standard value is −0.0054.

(3) The presented elements, AGQ6-I and AGQ6-II, possess high accuracy for all three mesh divisions, and are insensitive to three types of distortion. Moreover, they can even produce the exact solutions for the pure bending problem.

MacNeal [7] has pointed out that if the element can pass the constant strain/stress patch test in a finite size mesh (i.e., the strict patch test), the trapezoidal locking will inevitably appear for the element in the calculation of the MacNeal's thin beam. One reason that the present elements can successfully avoid trapezoidal locking is that the new tool of the quadrilateral area coordinate system is used, which can always keep the second-order completeness in Cartesian coordinates under distortion meshes. Besides, instead of the strict form, only the weak patch test are utilized in this paper (Example 8) to assure the convergence of the new elements.

Example 7. Cantilever beam divided by two elements containing a parameter of distortion (Fig. 10)

The cantilever beam shown in Fig. 10 is divided by two elements. The shape of the two elements varies with the distorted parameter e. When $e = 0$, both elements are rectangular. But with the increase of e, the mesh will be distorted more and more seriously. This is another famous benchmark for testing the sensitivity to the mesh distortion.

For pure bending problem, the results of the tip deflection at point A are listed in Table 9. Besides the present elements, the solutions obtained by other five models are also given for comparison.

From the Table 9, it shows that:

The accuracy of the element Q4 is the poorest. Its relative error reaches 72% when $e = 0$.

The accuracies of the elements QM6, P-S, QE2 and $\overline{B}$-Q4E are better than that of Q4. All these four elements can produce the exact solution when $e = 0$. But unfortunately, they are still sensitive to the mesh distortion. The relative error can reach 37% or so when $e = 1$, and will continue growing if e keeps increasing.

But the things become very different for the presented elements AGQ6-I and AGQ6-II. Both can keep providing the exact solutions when e varies from 0 to 5, i.e., they can overcome the trapezoidal locking completely. This shows again the advantages of the quadrilateral area coordinates and the weak patch test (Example 8).

Example 8. Weak patch test (Fig. 11)

The constant strain/stress weak patch test using irregular mesh is shown in Fig. 11. Let Young's modulus $E = 1000$, Poisson's ratio $\mu = 0.25$, and thickness of the patch $t = 1$. At first, the patch divided by only three elements, as shown in Fig. 11a, is considered. Each element is then bisected through the midpoints of the element sides. Thus, each original

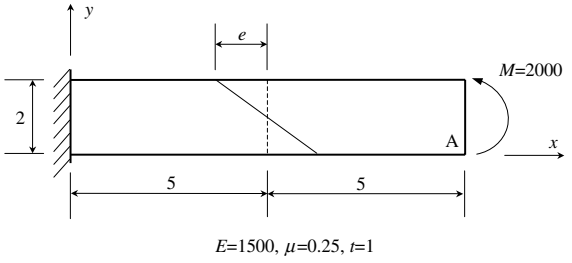

Fig. 10. Cantilever beam divided by two elements with distorted parameter e.

Table 9
Results of the tip deflection of a cantilever beam with a distorted parameter e (Fig. 10)

e	0	0.5	1	2	3	4	4.9
Q4	28.0	21.0	14.1	9.7	8.3	7.2	6.2
QM6	100	80.9	62.7	54.4	53.6	51.2	46.8
P-S	100	81.0	62.9	55.0	54.7	53.1	49.8
QE2	100	81.2	63.4	56.5	57.5	57.9	56.9
$\overline{B}$-Q4E	100	81.2	63.4	56.5	57.5	57.9	56.9
AQ6I	100	100	100	100	100	100	100
AQ6II	100	100	100	100	100	100	100
Exact	100	100	100	100	100	100	100

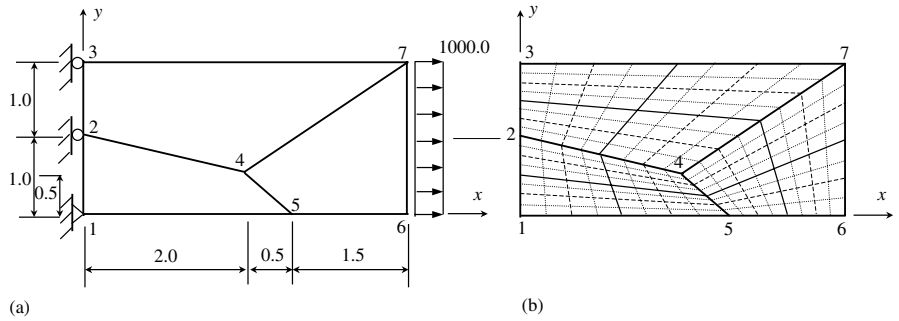

Fig. 11. Constant strain problem for weak patch test. (a) Three elements and (b) 192 elements.

Table 10
Weak patch test for element AQ6-I (Panel A), AQ6-II (Panel B)

Mesh	v_2	v_3	u_4	v_4	u_5	v_5	u_6	v_6	u_7	v_7
Panel A										
3 elements	−0.2787	−0.4291	2.0758	−0.4211	2.4946	−0.9491	5.4819	−0.8051	4.9589	−1.6375
12 elements	−0.2653	−0.4735	2.0508	−0.1862	2.4578	−0.3988	4.7955	0.1313	4.2688	−0.8346
48 elements	−0.2605	−0.4962	2.0142	−0.1238	2.4975	−0.1044	4.2432	0.1049	4.0753	−0.5683
192 elements	−0.2544	−0.4996	2.0042	−0.1231	2.5007	−0.0288	4.0685	−0.0383	4.0233	−0.5203
Exact	−0.2500	−0.5000	2.0000	−0.1250	2.5000	0.0000	4.0000	0.0000	4.0000	−0.5000
Panel B										
3 elements	−0.3010	−0.5017	1.7560	−0.8383	2.0800	−1.4505	5.0614	−2.1764	5.6885	−3.3179
12 elements	−0.2603	−0.4742	1.9686	−0.2532	2.4159	−0.4300	4.6898	−0.0461	4.3891	−1.0944
48 elements	−0.2592	−0.4952	1.9931	−0.1399	2.4883	−0.1126	4.2084	0.0563	4.1030	−0.6233
192 elements	−0.2540	−0.4992	1.9987	−0.1268	2.4988	−0.0314	4.0572	0.0242	4.0302	−0.5335
Exact	−0.2500	−0.5000	2.0000	−0.1250	2.5000	0.0000	4.0000	0.0000	4.0000	−0.5000

element is subdivided into four elements. Repeat this division again and again, the total number of the elements in the refined mesh after each action will be 12, 48, 192, ..., in turn. The mesh that contains 192 elements is plotted in Fig. 11b.

The results of nodal displacements u_i and v_i ($i = 2, 3, \ldots, 7$) in different mesh divisions, obtained by AGQ6-I and AGQ6-II, are shown in Table 10 panel A and panel B, respectively.

From Table 10 panel A and panel B, it can be seen that the new elements cannot give the exact solutions using the coarse mesh in finite size, i.e., they fail to pass the strict patch test. But with the subdivision of the mesh, the results obtained by both elements will converge to the exact solutions. Therefore, they pass the weak patch test.

It has to be acknowledged that in the constant strain/stress patch test the behavior of both present elements are not as perfect as in other foregoing examples, which are in fact more difficult patch tests. This phenomenon may be consistent with the theorem shown by MacNeal [7], i.e., four-node membrane elements with two DOFs per node would either lock in in-plane bending or fail to pass a C_0 patch test (strict form) when element shape is an isosceles trapezoid. However, since both elements can pass the weak constant strain/stress patch test, the convergence of these two non-conforming elements is still guaranteed.

It is not discovered in this paper, why the present elements fail to pass the strict form constant strain/stress patch test. It is worthy of further studies on this interesting topic. Some advanced concepts, for examples, the inf-sup tests proposed by Bathe [31,32], the convergence test for nonconforming elements proposed by Shi [33], etc., may be utilized to solve or explain the puzzle.

6. Conclusions

Two 4-node quadrilateral membrane elements, AGQ6-I and AGQ6-II, have been developed using the quadrilateral area coordinates and generalized conforming conditions. The formulations of these elements are quite simple

and easy to be constructed. And the potential accuracy and versatility of the said elements have been illustrated using eight numerical examples, which show that: the two new elements can not only produce the exact solutions for pure bending problems using arbitrary mesh, but also avoid trapezoidal locking of MacNeal's thin beam divided by distorted mesh. Compared with other 4-node quadrilateral membrane element models, the present elements exhibit higher precision and are more insensitive to mesh distortion. And their convergence is assured by passing the weak patch test.

The important significance of this paper is worthy of being pointed out:

(i) This paper provides successful experience for constructing quadrilateral membrane elements that are insensitive to mesh distortion. For a long time, many researchers have struggled for establishing effective element models that can not only solve the trapezoidal locking in MacNeal's thin beam problem, but also ensure the convergence of them. But after many failed attempts, somebody even suspected that above two purposes could not be achieved simultaneously. This paper negates this suspicion, because it is obviously that both purposes have been realized by the present elements. The success depends on two keys: the isoparametric coordinates are replaced by the quadrilateral area coordinate system; and the strict patch test is replaced by the weak form.

(ii) This paper also shows the advantages of the quadrilateral area coordinates, especially for their excellent performance that can improve insensitivity of elements to distorted meshes. This merit has been exhibited in Ref. [4] for constructing 8-node quadrilateral membrane elements, now it is again illustrated here for constructing 4-node models. Besides, the formulations expressed by the area coordinates are isotropic because the area coordinate system is a natural coordinate system. This is another distinguished character of the area coordinates, which the Cartesian coordinates cannot assure.

Acknowledgements

This study was supported by the Natural Science Foundation of China (project no. 10272063), the Basic Science Research Foundation of Tsinghua University (JC2002003), the Special Scientific Foundation for Chinese Doctoral Education (20020003044), and the Foundation for the Author of National Excellent Doctoral Dissertation of PR China (200242).

Appendix A. The subroutine of the element stiffness matrix (Fortran 90)

```
SUBROUTINE ELE_STIF_AGQ6(ESTIF, COREN, DMATX, T, ITYPE)

!*  ========================================                                    *!
!*  Variable Statement:                                                          *!
!*  A            :⇒ the Area of the quadrilateral element 1234                    *!
!*  A1, A2, A3   :⇒ the Areas of the triangle 124, 123 and 234, respectively      *!
!*  BLMATX(3,4)  :⇒ [Bλ], the strain MATriX of the internal DOFs                  *!
!*  BQMATX(3,8)  :⇒ [Bq], the strain MATriX of the external DOFs                  *!
!*  COREN(2,4)   :⇒ the COoRdinates of the Element Nodes                          *!
!*  DERIV_N(2,4) :⇒ the derivations of the shape function of the element Q4 respect to ξ, η *!
!*  DJACB        :⇒ the Jacobian determinant                                      *!
!*  DMATX(3,3)   :⇒ [D], the elastic MATriX of the element                        *!
!*  EITA(4)      :⇒ the isoparametric coordinates ηi (i = 1, 2, 3, 4) of the element nodes *!
!*  ESTIF(8,8)   :⇒ the Element STIFfness matrix [K]^e                            *!
!*  ESTIFLL(4,4) :⇒ [Kλλ], the second expression of Eq. (31)                      *!
!*  ESTIFLQ(4,8) :⇒ [Kλq], the third expression of Eq. (31)                       *!
!*  ESTIFQQ(8,8) :⇒ [Kqq], the first expression of Eq. (31)                       *!
!*  g(4)         :⇒ the four characteristic parameters of a quadrilateral         *!
!*  ITYPE        :⇒ the Indicator of the element TYPE,                            *!
!*                  ITYPE = 1: element AGQ6I; ITYPE = 2: element AGQ6II           *!
!*  KSAI(4)      :⇒ the isoparametric coordinates ξi (i = 1, 2, 3, 4) of the element nodes *!
```

```
!*   L(4)              :⇒ the area coordinates                                          *!
!*   N0X(4),N0Y(4)     :⇒ The derivations of nodal shape function respect to X, Y       *!
!*   NLX(2),NLY(2)     :⇒ The derivations of internal parameter shape function respect to X, Y *!
!*   POSGP(3)          :⇒ POSition of Gauss Points                                      *!
!*   SX, SY            :⇒ The expressions (Sx,Sy) in Eq. (26b), or (Sx,Sy) in Eq. (38b) *!
!*   T                 :⇒ the Thickness of the element                                  *!
!*   WEIGP(3)          :⇒ WEIght Coefficient of Gauss Points                            *!
!*   X(i)              :⇒ =COREN(1,i), the X-coordinates of the i-th node               *!
!*   XJACM(2,2)        :⇒ the JACOBI matrix of element Q4                               *!
!*   Y(i)              :⇒ =COREN(2,i), the Y-coordinates of the i-th node               *!
!*   = = = = = = = = = = = = = = = = = = = = = = = = = = = = = = = = = = = = = = = =   *!


IMPLICIT NONE
REAL*8, DIMENSION(8,8) :: ESTIF, ESTIFQQ
REAL*8, DIMENSION(4,4) :: ESTIFLL;  REAL*8, DIMENSION(4,8) :: ESTIFLQ
REAL*8, DIMENSION(3,4) :: BLMATX; REAL*8, DIMENSION(3,8) :: BQMATX
REAL*8, DIMENSION(3,3) :: DMATX;   REAL*8, DIMENSION(2,4) :: COREN, DERIV_N
REAL*8, DIMENSION(3)   :: POSGP, WEIGP; REAL*8, DIMENSION(2,2) :: XJACM
REAL*8, DIMENSION(4)   :: b, c, g, L,, X, Y, N0X, N0Y, NLX, NLY, KSAI, EITA
REAL*8 :: T ; INTEGER::ITYPE
REAL*8 :: A, A1, A2, A3, DJACB, DV, SX, SY
INTEGER:: i, j, k, ii, jj, kk, mm, igaus, jgaus

DO i=1, 4; X(i)=COREN(1,i); Y(i)=COREN(2,i); END DO
DO i=1,4                                    !\
  j=i+1; IF(j>4) j=1; k=j+1; IF(k>4) k=1    !| the second and third
  b(i)=Y(j)-Y(k); c(i)=X(k)-X(j)            !| formulae of Eq.(3)
END DO                                      !/

!*   The area of the triangle 124 (See Fig.2)------------------------------------   *!
  A1=0.5*(X(2)*Y(4)+X(1)*Y(2)+X(4)*Y(1)-X(2)*Y(1)- X(4)*Y(2)-X(1)*Y(4))
!*   The area of the triangle 123 (See Fig.2)------------------------------------   *!
  A2=0.5*(X(2)*Y(3)+X(1)*Y(2)+X(3)*Y(1)-X(2)*Y(1)- X(3)*Y(2)-X(1)*Y(3))
!*   The area of the triangle 234 (See Fig.2)-----------------------   *!
  A3=0.5*(X(3)*Y(4)+X(2)*Y(3)+X(4)*Y(2)-X(3)*Y(2)- X(4)*Y(3)-X(2)*Y(4))
!*   The area of the quadrilateral 1234 (See Fig.2)-----------------   *!
  A=A1+A3
!*   The characteristic parameters of a quadrilateral ---------------------------------   *!
  g(1)=A1/A; g(2)=A2/A; g(3)=1.0-g(1); g(4)=1.0-g(2) !Eq.(4)
!*   The positions and weight coefficients of Gauss points (3×3 case)-----------------   *!
  POSGP(1) = −0.774596669241483; POSGP(2)=0.0; POSGP(3) = −POSGP(1)
  WEIGP(1)= 0.555555555555556; WEIGP(2)=0.888888888888889; WEIGP(3)=WEIGP(1)
!*   The isoparametric coordinates (ξi, ηi) of the four element nodes------------------   *!
  KSAI(1) = −1.0; KSAI(2)=1.0; KSAI(3)=1.0; KSAI(4) = −1.0
  EITA(1) = −1.0; EITA(2) = −1.0; EITA(3)=1.0; EITA(4)= 1.0
!*   Initialize the element stiffness matrix to zero-----------------------------------   *!
  ESTIF=0.0; ESTIFQQ=0.0; ESTIFLL=0.0; ESTIFLQ=0.0
!*   Results of Eq.(33)----------------------------------------   *!
  LOOP1:DO igaus=1, 3
    LOOP2:DO jgaus=1, 3
!*   The area coordinates of the Gauss Points [See Eq.(7)]-------------------------   *!
  L(1)=0.25*(1.0-POSGP(igaus))*(g(2)*(1.0-POSGP(jgaus))+g(3)*(1.0+POSGP(jgaus)))
  L(2)=0.25*(1.0-POSGP(jgaus))*(g(4)*(1.0-POSGP(igaus))+g(3)*(1.0+POSGP(igaus)))
```

```
L(3) = 0.25*(1.0+POSGP(igaus))*(g(1)*(1.0-POSGP(jgaus))+g(4)*(1.0+POSGP(jgaus)))
L(4) = 0.25*(1.0+POSGP(jgaus))*(g(1)*(1.0-POSGP(igaus))+g(2)*(1.0+POSGP(igaus)))

!*   The strain matrix of the external DOFs [See Eq.(24)]---------- ----------  *!
BQMATX = 0.0
LOOP3: DO i = 1,4
 j = i+1; IF(j>4) j = 1; k = j+1; IF(k>4) k = 1
 SX = 0.0; SY = 0.0
 LOOP4: DO ii = 1,4
    jj = ii+1; IF(jj>4) jj = 1; kk = jj+1; IF(kk>4) kk = 1; mm = kk+1; IF(mm>4) mm = 1
    SELECT CASE(ITYPE)
       CASE(1)
          SX = SX+b(ii)*KSAI(ii)*EITA(ii)*(3.0*(L(jj)-L(mm))+(g(jj)-g(kk)))      !\
          SY = SY+c(ii)*KSAI(ii)*EITA(ii)*(3.0*(L(jj)-L(mm))+(g(jj)-g(kk)))      !/ Eq. (26b)
       CASE(2)
          SX = SX+b(ii)*KSAI(ii)*EITA(ii)*(L(jj)-L(mm))                          !\
          SY = SY+c(ii)*KSAI(ii)*EITA(ii)*(L(jj)-L(mm))                          !/ Eq. (38b)
    END SELECT
 END DO LOOP4
 SELECT CASE(ITYPE)
    CASE(1)
       N0X(i) = (b(i)+b(j))/A/2.0 &                                              !\
                +KSAI(i)*EITA(i)*g(k)*SX/2.0/A/(1.0+g(1)*g(3)+g(2)*g(4))         !|
       N0Y(i) = (c(i)+c(j))/A/2.0 &                                              !| Eq. (26a)
                +KSAI(i)*EITA(i)*g(k)*SY/2.0/A/(1.0+g(1)*g(3)+g(2)*g(4))         !/
    CASE(2)
       N0X(i) = (b(i)+b(j))/A/2.0 &                                              !\
                +KSAI(i)*EITA(i)*g(k)*SX/2.0/A/(g(1)*g(3)+g(2)*g(4))             !|
       N0Y(i) = (c(i)+c(j))/A/2.0 &                                              !| Eq. (38a)
                +KSAI(i)*EITA(i)*g(k)*SY/2.0/A/(g(1)*g(3)+g(2)*g(4))             !/
 END SELECT
 BQMATX(1,2*i-1) = N0X(i); BQMATX(2,2*i) = N0Y(i)                                !\
 BQMATX(3,2*i-1) = BQMATX(2,2*i); BQMATX(3,2*i) = BQMATX(1,2*i-1) !/ Eq. (25)
END DO LOOP3

!*   The strain matrix of the internal DOFs [See Eq. (27)]----------–---------- *!
BLMATX = 0.0
LOOP5: DO i = 1,2
 j = i+1; IF(j>4) j = 1; k = j+1; IF(k>4) k = 1
 NLX(i) = (b(i)*L(k)+b(k)*L(i))/A/2.0; NLY(i) = (c(i)*L(k)+c(k)*L(i))/A/2.0    ! Eq. (29)
 BLMATX(1,2*i-1) = NLX(i); BLMATX(2,2*i) = NLY(i)                              !
 BLMATX(3,2*i-1) = BLMATX(2,2*i); BLMATX(3,2*i) = BLMATX(1,2*i-1) !/ Eq. (28)
END DO LOOP5

!*   The derivations of the shape function of the element Q4 respect to ξ, η at the Gauss points --------  *!
DERIV_N(1,1) = -0.25*(1.0-POSGP(jgaus)); DERIV_N(1,2) = 0.25*(1.0-POSGP(jgaus))
DERIV_N(1,3) = 0.25*(1.0+POSGP(jgaus)); DERIV_N(1,4) = -0.25*(1.0+POSGP(jgaus))
DERIV_N(2,1) = -0.25*(1.0-POSGP(igaus)); DERIV_N(2,2) = -0.25*(1.0+POSGP(igaus))
DERIV_N(2,3) =  0.25*(1.0+POSGP(igaus)); DERIV_N(2,4) =  0.25*(1.0-POSGP(igaus))

!*   The JACOBI matrix and its determinant of element Q4-------–----------  *!
XJACM = MATMUL(DERIV_N,TRANSPOSE(COREN))
DJACB = XJACM(1,1)*XJACM(2,2)-XJACM(1,2)*XJACM(2,1)
!*   Calculate Eq. (33)---------- ----------  *!
DV = DJACB*WEIGP(igaus)*WEIGP(jgaus)*T
ESTIFQQ = ESTIFQQ+DV*MATMUL(TRANSPOSE(BQMATX), MATMUL(DMATX,BQMATX))
ESTIFLL = ESTIFLL+DV*MATMUL(TRANSPOSE(BLMATX), MATMUL(DMATX,BLMATX))
```

```
    ESTIFLQ = ESTIFLQ+DV*MATMUL(TRANSPOSE(BLMATX), MATMUL(DMATX,BQMATX))
    END DO LOOP2
  END DO LOOP1
  !*    Call Subroutine BRINV to calculate the inverse matrix of the matrix ESTIFLL ([Kλλ]----------    *!
    CALL BRINV(ESTIFLL,4) ! ESTIFLL becomes its inverse matrix after BRINV
  !*    Calculate the element stiffness matrix [Eq. (30)]----------------------------------------    *!
    ESTIF = ESTIFQQ-MATMUL(TRANSPOSE(ESTIFLQ), MATMUL(ESTIFLL,ESTIFLQ))
  END SUBROUTINE ELE_STIF_AGQ6

  !*    = = = = = = = = = = = = = = = = = = = = = = = = = = = = = = = = = = = = = = = = = = = = = = = = = = = = = = = = *!
  !*    !*Subroutine BRINV: Solve the inverse matrix of a N-order square matrix [A] by                                *!
  !*                              complete pivot Gauss-Jordan elimination *!*!                                        *!
  !*    = = = = = = = = = = = = = = = = = = = = = = = = = = = = = = = = = = = = = = = = = = = = = = = = = = = = = = = = *!

  SUBROUTINE BRINV(A,N)
    REAL*8,DIMENSION(N,N):: A; INTEGER,DIMENSION(N)::IS,JS
    REAL*8 ::D,T; INTEGER::I,J,L,K,N
     L = 1
     LOOP1: DO K = 1,N
        D = 0.0
        LOOP2: DO I = K,N
           DO J = K,N; IF(ABS(A(I,J)) > D) THEN; D = ABS(A(I,J)); IS(K) = I; JS(K) = J; END IF; END DO
        END DO LOOP2
        IF(D = = 0.0) THEN; L = 0; WRITE(*,'(1X,A)')'ERROR IN BRINV**NOT INV'; STOP; END IF
        DO J = 1,N; T = A(K,J); A(K,J) = A(IS(K),J); A(IS(K),J) = T; END DO
        DO I = 1,N; T = A(I,K); A(I,K) = A(I,JS(K)); A(I,JS(K)) = T; END DO
        A(K,K) = 1.0/A(K,K)
        DO J = 1,N; IF(J/ = K) THEN; A(K,J) = A(K,J)*A(K,K); END IF; END DO
        LOOP3: DO I = 1,N
           IF(I/ = K) THEN
              DO J = 1,N; IF(J/ = K) THEN; A(I,J) = A(I,J)-A(I,K)*A(K,J); END IF; END DO
           END IF
        END DO LOOP3
        DO I = 1,N; IF(I/ = K) THEN; A(I,K) = -A(I,K)*A(K,K); END IF; END DO
     END DO LOOP1
    LOOP4: DO K = N,1,-1
     DO J = 1,N; T = A(K,J); A(K,J) = A(JS(K),J); A(JS(K),J) = T; END DO
     DO I = 1,N; T = A(I,K); A(I,K) = A(I,IS(K)); A(I,IS(K)) = T; END DO
    END DO LOOP4
  END SUBROUTINE BRINV
```

References

[1] Lee NS, Bathe KJ. Effects of element distortion on the performance of isoparametric elements. Int J Numer Meth Engng 1993;36:3553–76.

[2] Long YQ, Li JX, Long ZF, Cen S. Area coordinates used in quadrilateral elements. Commun Numer Meth Engng 1999;19(8):533–45.

[3] Long ZF, Li JX, Cen S, Long YQ. Some basic formulae for Area coordinates used in quadrilateral elements. Commun Numer Meth Engng 1999;19(12):841–52.

[4] Soh AK, Long YQ, Cen S. Development of eight-node quadrilateral membrane elements using the area coordinates methods. Comput Mech 2000;25(4):376–84.

[5] Soh AK, Long ZF, Cen S. Development of a new quadrilateral thin plate element using area coordinates. Comput Meth Appl Mech Engng 2000;190(8–10):979–87.

[6] MacNeal RH, Harder RL. A proposed standard set of problems to test finite element accuracy. Finite Elements Anal Design 1985;1:3–20.

[7] MacNeal RH. A theorem regarding the locking of tapered four-noded membrane elements. Int J Numer Meth Engng 1987;24:1793–9.

[8] Wilson EL, Taylor RL, Doherty WP, Ghabussi T. Incompatible displacement models. In: Fenven ST et al., editors. Numerical and Computer Methods in Structural Mechanics. New York: Academic Press; 1973. p. 43–57.
[9] Taylor RL, Beresford PJ, Wilson EL. A non-conforming element for stress analysis. Int J Numer Meth Engng 1976;10:1211–9.
[10] Pian THH, Sumihara K. Rational approach for assumed stress finite elements. Int J Numer Meth Engng 1984;20:1685–95.
[11] Pian THH, Wu CC. General formulation of incompatible shape function and an incompatible isoparametric element. Proceedings of the Invitational China–American Workshop on FEM, Chengde, China, 1986. p. 159–65.
[12] Chen WJ, Cheung YK. Three dimensional 8-node and 20-node refined hybrid isoparametric elements. Int J Numer Meth Engng 1992;35:1871–89.
[13] Chen WJ, Tang LM. Isoparametric quasi-conforming element. J Dalian Univ Technol 1981;20(1):63–74 [in Chinese].
[14] Andelfinger U, Ramm E. EAS-elements for two-dimensional, three-dimensional, plate and shell structures and their equivalence to HR-elements. Int J Numer Meth Engng 1993;36:1311–37.
[15] Piltner R, Taylor RL. A systematic constructions of B-bar functions for linear and nonlinear mixed-enhanced finite elements for plane elasticity problems. Int J Numer Meth Engng 1997;44:615–39.
[16] Irons BM, Razzaque A. Experience with patch test for convergence of finite element methods. In: Aziz AK, editor. Mathematical Foundations of the Finite Element Methods. Academic Press; 1972. p. 557–87.
[17] Bazeley GP, Cheung YK, Irons BM, Zienkiewicz OC. Triangular elements in bending—conforming and non-conforming solutions. Proc Conf Matrix Methods in Structural Mechanics. Ohio, 1965.
[18] Zienkiewicz OC, Taylor RL. In: The finite element method. 5th ed. The basis, vol. 1. Oxford: Butterworth-Heinnemann; 2000.
[19] Strang G, Fix GJ. An analysis of the finite element method. Englewood Cliffs: Prentice-Hall; 1973.
[20] Stummel E. The limitation of the patch test. Int J Numer Meth Engng 1980;15:177–88.
[21] Shi ZC. An explicit analysis of Stummel's patch test examples. Int J Numer Mech Engng 1984;20:1233–46.
[22] Cook RD, Malkus DS, Plesha ME. Concepts and applications of finite element analysis. 3rd ed. New York: John Wiley & Sons Inc.; 1989.
[23] Long YQ, Xin KG. Generalized conforming elements for bending and bucking analysis of plates. Finite Elements Anal Design 1989;5:15–30.
[24] Long YQ, Bu XM, Long ZF, Xu Y. Generalized conforming plate bending elements using point and line compatibility conditions. Comput Struct 1995;54(4):717–23.
[25] Long YQ, Xu Y. Generalized conforming quadrilateral membrane element with vertex rigid rotational freedom. Comput Struct 1994;52(4):749–55.
[26] Long YQ, Xu Y. Generalized conforming triangular membrane element with vertex rigid rotational freedom. Finite Elements Anal Design 1994;17:259–71.
[27] Cook RD. Improved two-dimension finite element. J Struct Div, ASCE 1974;100ST9:1851–63.
[28] Bassayya K, Bhattacharya K, Shrinivasa U. Eight-node brick, PN340, representing constant stress fields exactly. Comput Struct 2000;74:441–60.
[29] Ibrahimgovic A, Taylor RL, Wilson EL. A robust quadrilateral membrane element with rotational degrees of freedom. Int J Numer Meth Engng 1990;30:445–57.
[30] MacMeal RH, Harder RL. A refined four-noded membrane element with rotation degrees of freedom. Comput Struct 1988;28(1):75–84.
[31] Bathe KJ. The inf-sup condition and its evaluation for mixed finite element methods. Comput Struct 2001;79:243–52.
[32] Pantuso D, Bathe KJ. A four-node quadrilateral mixed-interpolated element for solids and fluids. Math Models Meth Appl Sci 1995;5(8):1113–28.
[33] Shi ZC. The F-E-M-Test for convergence of nonconforming finite elements. Math Comput 1987;49(180):391–405.